An *Eulerian-like* interface-capturing approach for modeling the fouling process by crystallization

Andrés M. Nieves Chacón[1], Renato S. Silva[1], Regina C. Almeida[1]

[1]*National Laboratory for Scientific Computing*
Av. Getúlio Vargas - 333, CEP 25651-075, Petrópolis/RJ, Brazil
andresmn@posgrad.lncc.br, rssr@lncc.br, rcca@lncc.br

Abstract. This study introduces a new strategy for capturing the interface between water and the fouling layer on heat transfer surfaces. This approach fits within moving boundary problems and is referred to as an *Eulerian-like* Interface-Capturing Approach for Modeling the Fouling Process by Crystallization (ELICAFC). Fouling is a prevalent industrial phenomenon characterized by the deposition of undesirable compounds on heat transfer surfaces. Several mathematical models have been proposed in the literature to predict the average fouling growth over time, with one of the key challenges being the tracking or capturing of the fouling layer's interface. In this context, capturing the fouling layer movement not only aids in estimating the increase in thermal resistance but also in controlling heat transfer efficiency over space and time. The Finite Element Method is employed within the ELICAFC strategy, utilizing the Bohnet model to estimate the net deposition rate resulting from the crystallization process. The ELICAFC procedure is used to estimate temperature distribution, fouling growth, and thermal resistance in an idealized fouling scenario. Numerical results align with the expected physical behavior and verify the consistency of the ELICAFC approach.

Keywords: Crystallization fouling, Interface-capturing, Moving boundary problems

1 Introduction

Heat exchangers constitute prevalent devices in several industrial processes, facilitating efficient heat transfer between two or more fluids. However, undesirable compounds deposited on the heat exchanger walls generate the so-called fouling phenomenon, which has addressed new challenges regarding the evolution of the fouling-liquid layer interface over space-time. These issues are studied within the field of moving boundary problems (MBPs). According to Wörner [1], interface-tracking and interface-capturing methods represent a category of MBPs, involving Lagrangian and Eulerian approaches, respectively. The MBPs can be conducted using the Finite Element Method (FEM) or the Finite Volume Method (FVM). As Donea et al. [2] indicated, in the Lagrangian scheme specific mesh nodes track each corresponding material particle during movement, which makes that pure Lagrangian applications entail high computational costs because of the required mesh updating and remeshing processes. From the Eulerian perspective, the interface is captured using a fixed grid, rendering the construction of new meshes unnecessary as the interface evolves.

The *Volume-of-Fluid* (VOF) and the *Level-set* (LS) methods are widely used Eulerian techniques in MBPs, primarily utilized to simulate the evolution of two-phase immiscible flows. Both techniques aim to solve a convection-diffusion equation, where a parameter ϕ denotes a fluid volume fraction in the case of the VOF method, with the interface being implicitly captured in the $0 < \phi < 1$. As mentioned by Malú Grave et al. [3], the LS method advects a transport function ϕ and segregates two phases using signed distance functions (SDFs), with the interface depicted by the zero level-set ($\phi = 0$). In contrast, hybrid methods have been developed to integrate both Lagrangian and Eulerian formulations. As presented by Donea et al. [2], the Arbitrary Lagrangian-Eulerian (ALE) methods are the most popular hybrid alternatives for MBPs. These methods include mesh updating, mesh adaptation, and node movements as the simulation unfolds. The fouling phenomenon encompasses a solid-liquid interface, represented by the boundary Γ_{fl}. In this line, Kasper et al. [4] employed a Lagrangian-Eulerian approach, where the fluid was treated as a continuum medium from an Eulerian reference frame, typically incorporating a turbulence model. Moreover, the fouling particles are tracked from a Lagrangian viewpoint, considering drag, lift, and gravitational forces. Hence, the VOF or LS methods are not commonly applied in fouling problems and pure Lagrangian alternatives are often considered too computationally expensive. Hybrid methods have been useful for tackling fouling problems, but commonly they also require remeshing.

In this work, we propose a straightforward numerical alternative that differs from the aforementioned strategies in the following aspects: the interface is not captured by implicitly transporting it, as in VOF or LS methods, but rather by employing a crystallization model. In this case, fouling growth is estimated using the Bohnet model, and the interface Γ_{fl} moves accordingly. Despite the movement of the mesh nodes due to fouling growth, ELICAFC does not require remeshing. This alternative approach deviates from pure Eulerian methods due to the dynamic movement of mesh nodes. We call this strategy as an *Eulerian-like* interface-capturing approach for modeling the fouling process by crystallization (ELICAFC). Since the ELICAFC implementation incorporates space-time interactions, it enables heat transfer analysis by providing estimates of thermal resistance and the control of heat transfer efficiency. The ELICAFC strategy is implemented in a proposed general scenario to assess its feasibility from a numerical perspective and its alignment with expected physical behavior. The validation phase, incorporating experimental data, is planned for future works. The temperature evolution of both the fouling-liquid and fouling-wall interfaces along the pipe domain are analyzed, the fouling growth and the resistance of the fouling layer are estimated. In section 2, we present the simulation methodology by integrating the heat and fouling mathematical models, and outlining the computational implementation. The features and the procedure of the ELICAFC strategy are detailed in section 3. In section 4, we discuss the results of the ELICAFC application. Finally, conclusions and suggestions for future work are summarized in section 5.

2 Simulation methodology

The scenario of interest consists of hot and cold water flows outside and inside a cylindrical tube, respectively. Figure 1 depicts the pipe domain from its axisymmetric view for a certain n-th time step. The domain Ω consists of subdomains Ω_w, Ω_f, and Ω_l, corresponding to the heat exchanger wall, the fouling layer, and the liquid water. Each one has associated its corresponding boundary, where $\partial\Omega_{wl}$ and $\partial\Omega_{wr}$ correspond to the left and right boundaries of the wall, $\partial\Omega_{fl}$ and $\partial\Omega_{fr}$ are the left and right boundaries of fouling, and $\partial\Omega_l$ is the boundary of the water subdomain. The internal boundaries Γ_{fl} and Γ_{fw} respectively represent the interfaces of the fouling-liquid layer and the fouling-wall. The parameters r_{in} and r_o correspond to the inner and outer radii, respectively. The remaining symbols in Fig.1 will be explained in subsequent sections. All thermophysical parameters involved within the heat and crystallization models are summarized in Table 1.

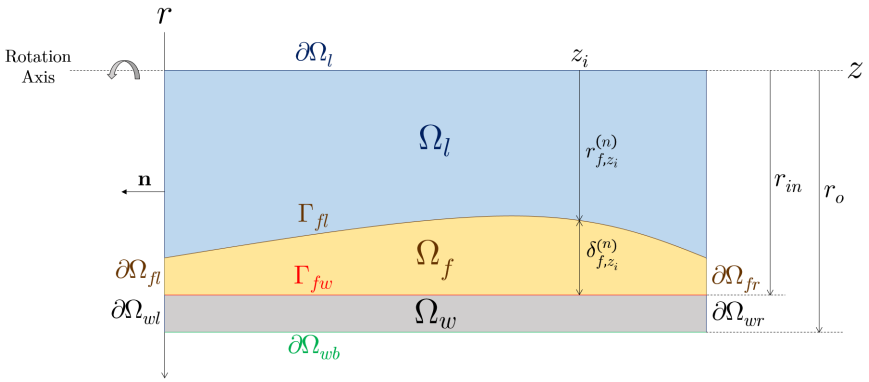

Figure 1. An schematic view of the domain of the fouling problem, where $r^{(n)}_{f,z_i}$ and $\delta^{(n)}_{f,z_i}$ are the radius and thickness of fouling at position z_i and time n

2.1 The heat transfer model

Let us consider $\Omega \subset \mathbb{R}^2$ with an exterior normal vector $\mathbf{n}$ and $T = (0, t_\infty]$ as the spatial and temporal domains, respectively. The heat transfer problem involves finding the temperature distribution field $\theta(r, z, t) \in C^2(\Omega \times T)$, such that

$$\mathbb{D}_\rho \mathbb{C}_p \frac{\partial}{\partial t}(\theta(r,z,t)) - \operatorname{div}(\mathbb{K}\nabla\theta(r,z,t)) = 0, \quad \text{in} \quad (\Omega_w \cup \Omega_f) \times T \tag{1}$$

$$\theta(r,z,0) = \theta_\infty, \quad (r,z) \in \Omega \backslash \partial\Omega_{wb} \tag{1a}$$

$$\theta(r,z,0) = \theta_{wb}, \quad (r,z) \in \partial\Omega_{wb} \tag{1b}$$

$$-(\mathbb{K}\boldsymbol{\nabla}\theta(r,z,0)\cdot\mathbf{n} = h(r^{(0)}_{f,z_i}(\theta_{fl}))(\theta(r,z,0) - \theta_\infty), \quad (r,z) \in \Gamma_{fw} \tag{1c}$$

$$\theta(r,z,t) = \theta_\infty, \quad (r,z,t) \in \overline{\Omega}_l \times T \tag{1d}$$

$$\theta(r,z,t) = \theta_{wb}, \quad (r,z,t) \in \partial\Omega_{wb} \times T \tag{1e}$$

$$-\mathbb{K}\boldsymbol{\nabla}\theta(r,z,t)\cdot\mathbf{n} = 0, \quad (r,z,t) \in \partial\Omega_{frl} \times T \tag{1f}$$

$$-(\mathbb{K}\boldsymbol{\nabla}\theta(r,z,t))\cdot\mathbf{n} = h(r^{(n)}_{f,z_i}(\theta_{fl}))(\theta(r,z,t) - \theta_\infty), \quad (r,z,t) \in \Gamma_{fl} \times T. \tag{1g}$$

Equation (1) represents the governing heat transfer equation, while equations (1a) and (1b) denote initial conditions. Specifically, eq. (1a) is imposed on entire domain excluding the boundary $\partial\Omega_{wb}$, while eq. (1b) is imposed on $\partial\Omega_{wb}$. Equation (1c) represents an initial convection condition where the fouling-wall interface (Γ_{fw}) interacts with water at $t = 0$. Equation (1e) represents a Dirichlet boundary condition, eq. (1f) represents Neumann boundary conditions applied on the left and right boundaries of both fouling and wall subdomains, where $\partial\Omega_{frl} = (\partial\Omega_{fr} \cup \partial\Omega_{fl} \cup \partial\Omega_{wr} \cup \partial\Omega_{wl})$. A Robin boundary condition is applied on the moving boundary Γ_{fl} as described in eq. (1g). The model operates under the following assumptions: **(1)** the water temperature θ_∞ will be kept constant throughout the simulation. Consequently, the temperature values in Ω_l and $\partial\Omega_l$ are equal to θ_∞, as described in eq. (1d); **(2)** the thermal conductivity $\mathbb{K}$, the density $\mathbb{D}_\rho$, and the specific heat $\mathbb{C}_p$ remains constant for the wall and fouling subdomains,

$$\mathbb{K} = \begin{cases} k_w, & \text{in} \quad \Omega_w \\ k_f, & \text{in} \quad \Omega_f \end{cases}, \quad \mathbb{D}_\rho = \begin{cases} \rho_w, & \text{in} \quad \Omega_w \\ \rho_f, & \text{in} \quad \Omega_f \end{cases}, \quad \mathbb{C}_p = \begin{cases} c_{pw}, & \text{in} \quad \Omega_w \\ c_{pf}, & \text{in} \quad \Omega_f; \end{cases} \tag{2}$$

(3) the left and right boundaries of both the pipe and fouling domains are considered insulated, as described in eq. (1f). Regarding the fouling lateral boundaries, although they are in contact with water, they are treated as insulated to prevent results that might perturb the temperature distribution on both sides, and **(4)** the flow is rotationally symmetric in z-direction. This assumption has been assumed elsewhere, as considered by Babuška et al. [5].

In this model, θ_{wb} is the wall temperature at the outer heat exchanger case denoted by the $\partial\Omega_{wb}$ boundary. The convection heat transfer coefficient $h(r^{(n)}_{f,z_i}(\theta_{fl}))$ depends on the fouling radius $r^{(n)}_{f,z_i}(\theta_{fl})$, where $\theta_{fl} = \theta(r, z, t(n)), (r, z) \in \Gamma_{fl}$. While the fouling radius depends on other parameters defined in the ensuing subsection, only θ_{fl} varies over time. The Nusselt correlation proposed by Bhatti and Shah, as gathered by Rohsenow et al. [6], is employed to estimate $h(r^{(n)}_{f,z_i}(\theta_{fl}))$. This coefficient also depends on the friction factor, which is estimated using the Haaland correlation gathered by Rohsenow et al. [6].

2.2 The crystallization fouling model

According to Bohnet [7], the rate of the total mass per unit area contained on a heat transfer surface at time $t(n)$, denoted as $\dot{m}^{(n)}_{f,z_i}$, is defined as the difference between the deposited $\dot{m}^{(n)}_{d,z_i}$ and removed $\dot{m}^{(n)}_{r,z_i}$, $\dot{m}^{(n)}_{f,z_i} = \dot{m}^{(n)}_{d,z_i} - \dot{m}^{(n)}_{r,z_i}$. The mass deposition rate is given by,

$$\frac{dm^{(n)}_{d,z_i}}{dt} = \beta(r^{(n)}_{f,z_i}(\theta_{fl})) \left\{ \frac{\beta(r^{(n)}_{f,z_i}(\theta_{fl}))}{2\eta(\theta_{fl})} + (c_F - c_s) - \sqrt{\frac{\beta^2(r^{(n)}_{f,z_i}(\theta_{fl}))}{4\eta^2(\theta_{fl})} + \frac{\beta(r^{(n)}_{f,z_i}(\theta_{fl}))}{\eta(\theta_{fl})} \cdot (c_F - c_s)} \right\}, \tag{3}$$

where the parameters β, η, c_F are respectively the mass transfer coefficient, the rate of reaction, and the bulk concentration of $CaCO_3$. The mass removal rate per unit area is estimated similarly to that defined in the Bohnet model as

$$\frac{dm^{(n)}_{r,z_i}}{dt} = \frac{1}{P/K_6}\, c_d\, \rho_f \left(\sqrt[3]{\rho_l^2 \mu_l g} \right) \delta^{(n)}_{f,z_i}(r^{(n)}_{f,z_i}(\theta_{fl}))\, v^2, \tag{4}$$

where the ratio P/K_6 is the same defined by Bohnet [7] and v is the velocity of the water. The fouling thickness $\delta^{(n)}_{f,z_i}(r^{(n)}_{f,z_i}(\theta_{fl}))$ is the difference between the inner and fouling radii at the n-th time step, $\delta^{(n)}_{f,z_i}(r^{(n)}_{f,z_i}(\theta_{fl})) = r_{in} - r^{(n)}_{f,z_i}(\theta_{fl})$. Finally, the average fouling radius is determined at each nodal value along z-direction, considering the size of the time step Δt as

$$r^{(n)}_{f,z_i}(\theta_{fl}) = \sqrt{\left(r^{(n-1)}_{f,z_i}(\theta_{fl})\right)^2 - \frac{2\dot{m}^{(n)}_f(r^{(n-1)}_{f,z_i}(\theta_{fl}))\Delta t}{\rho_f}}. \tag{5}$$

As the fouling layer increases, the thermal resistance to the heat transfer also increases. This effect is quantified by the fouling factor $R^{(n)}_{f,z_i}(r^{(n)}_{f,z_i}(\theta_{fl})) = (1/k_f)(r^{(n)}_{f,z_i}(\theta_{fl}))\ln(r_{in}/r^{(n)}_{f,z_i}(\theta_{fl}))$, and the average of the fouling resistance $\overline{R^{(n)}_f}$ along z-direction is approximated by $\overline{R^{(n)}_f} = (1/N)\sum_{i=1}^{N} R^{(n)}_{f,z_i}$, where N denotes the number of discretized nodes in z-direction according to the computational mesh. In this model, the thermophysical properties and the water velocity will be maintained constant.

2.3 Computational implementation

The computational domain consists of a structured grid, with triangular elements used for the heat exchanger wall and quadrilateral elements employed for the fouling-liquid region. Triangular elements were chosen for the heat exchanger wall to reduce computational costs, as they require fewer operations than quadrilaterals. On the other hand, quadrilateral elements were used for the rest of the domain (fouling and water) to facilitate control of fouling growth, as detailed in section 3. All experiments were conducted utilizing the classical Galerkin method with linear interpolation. The spatial and time variables were discretized using FEM and the backward Euler method, respectively. The finite element mesh was generated using the *ANSYS mesh* generator, and has 9625 elements with one degree of freedom. The implementation was executed using the Python programming language, where sparse *linalg* (linear algebra) Python functions were used for solving the linear system of equations. Specifically, a *Super Incomplete LU factorization* was employed as a preconditioner applying the conjugate gradient method, as described in Barrett et al. [8]. The heat transfer model exhibits nonlinearity due to the convective heat transfer coefficient in eq. (1g), which depends on the fouling radius over time. The nonlinear problem is solved using the fixed-point iterative method. Spurious solutions can arise due to the boundary condition established in eq. (1g), whose application varies spatially because of the Γ_{fl} movement. To mitigate these nonphysical solutions, the *Pearson* method was implemented during the initial time step, as documented by Arruda et al. [9].

3 The ELICAFC strategy

The ELICAFC strategy aims to capture the Γ_{fl} interface by employing an *Eulerian-like* reference frame. This is carried out using a background mesh, where the nodes linked to the Γ_{fl} interface are gradually moved according to the increase of the fouling layer. Nodes not linked to the fouling layer have a prescribed value corresponding to the water temperature at each time step, as defined in eq. (1d). In addition to the discretization of the wall using triangular elements, the background mesh discretizing $(\Omega_w \cup \Omega_f)$ consists of $a \times b$ elements along the z and r directions denoted by E_m^s, with $m = 1, \ldots, a$ and $s = 1, \ldots, b$. Mesh nodes belonging to Γ_{fl} are moved vertically to ensure that no mesh updating is necessary. This is implemented by defining a control parameter, denoted by $\alpha_m^{(n)}$, that indicates the number of elements in the m-th column of the mesh occupied by fouling at each n-th time step. This control parameter is defined as $\alpha_m^{(n)} = \lceil A_{f_m}/A_{ref} \rceil$, where $\lceil \cdot \rceil$ is the ceiling function. The quadrilateral reference area is $A_{ref} = \Delta z \Delta r$ and A_{f_m} is the accumulated area occupied by fouling at each m-th column, approximated by $A_{f_m} = ((d_m^{left} + d_m^{right})/2)\Delta z$. Here, d_m^{left} and d_m^{right} represent the accumulated fouling thickness at the left and right sides of each m-th column, with $d_m^{left} = \delta_{f,z_i}^{(n)}(r_{f,z_i}^{(n)})$ and $d_m^{right} = \delta_{f,z_{i+1}}^{(n)}(r_{f,z_{i+1}}^{(n)})$, for each i-th discretized node along z-direction. Figure 2 summarizes an example of the ELICAFC process over six time steps for a single m-th column, considering $A_{ref} = 1$. For simplicity, it is assumed that the fouling thickness grows uniformly along z-direction, $d_m^{left} = d_m^{right}$. Quadrilateral elements associated with the fouling layer and the water are respectively indicated in orange and blue. The moving nodes correspond to those situated at the top face of the element in the p_m-th position, associated with the r-direction, whose coordinates are denoted by $r_{p_m,i}^{\text{TOP}}$.

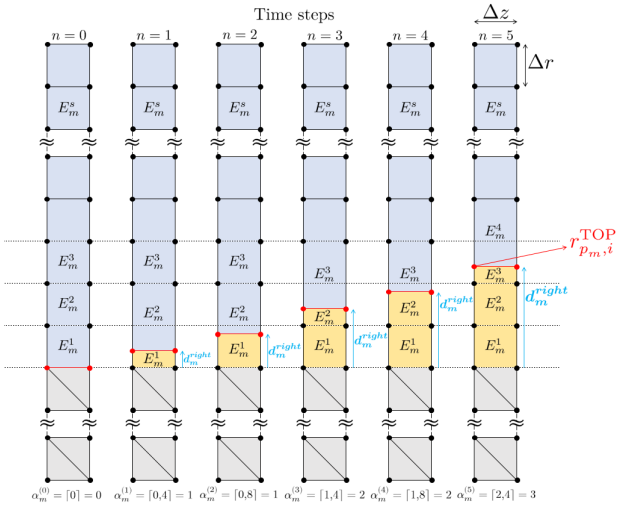

Figure 2. Example of the ELICAFC strategy over six-time steps for a single m-th column of the background mesh

The position p_m is determined by the $\alpha_m^{(n)}$ value, indicating the element of the backgound mesh whose top nodes coordinates are changed to follow Γ_{fl}. At the initial time step $\alpha_m^{(0)} = 0$, indicating that the Γ_{fl} interface is

equal to the Γ_{fw} interface (left column in Fig. 2). Assuming that in the next step the A_{f_m}/A_{ref} ratio is equal to 0.4, $\alpha_m^{(0)} = \lceil 0.4 \rceil = 1$, meaning that the fouling layer consists of one element (E_m^1, $p_m = 1$) whose top nodes $r_{1,i}^{\mathrm{TOP}}$ and $r_{1,i+1}^{\mathrm{TOP}}$ were moved to the fouling thickness, $r_{1,i}^{\mathrm{TOP}} = r_{in} - \delta_{f,z_i}^{(0)} = r_{f,z_i}^{(0)}$ and $r_{1,i+1}^{\mathrm{TOP}} = r_{in} - \delta_{f,z_{i+1}}^{(0)} = r_{f,z_{i+1}}^{(0)}$. After two more time steps, $\alpha_m^{(3)} = \lceil 1.4 \rceil = 2$, so that the fouling layer now consists of two elements. This implies that $p_m = 2$ and the top face of E_m^2 is the current Γ_{fl} and their coordinates were moved to, $r_{2,i}^{\mathrm{TOP}} = r_{f,z_i}^{(3)}$ and $r_{2,i+1}^{\mathrm{TOP}} = r_{f,z_{i+1}}^{(3)}$. Note that from $n = 1$ to $n = 2$, the top nodes of E_m^1 are moved up to track the increase of d_m^{right}. In the subsequents two time steps, the displaced nodes correspond to the top nodes of E_m^2 and at $n = 5$, $\alpha_m^{(5)} = p_m = 3$, with fouling layer encompassing E_m^1 , E_m^2 and E_m^3. Algorithm 1 presents a pseudocode to reproduce the ELICAFC strategy.

Algorithm 1 ELICAFC procedure

Initialization: $r_{f,z_i}^{(0)} \leftarrow r_{in}, \forall i = 1, \ldots, a+1$; $\alpha_m^{(0)} \leftarrow 0$, $p_m \leftarrow \alpha_m^{(0)}, \forall m = 1, \ldots, a$; $n_{steps} \leftarrow t_\infty/\Delta t$
for $n = 1$ to $n = n_{steps}$ **do**
  Find the temperature field $\theta(r, z, t)$
  $\theta_{fl} \leftarrow \theta(r, z), \forall (r, z) \in \Gamma_{fl}$
  $\eta(\theta_{fl}) \leftarrow \eta_0 \exp\left(-\dfrac{E}{R\,\theta_{fl}}\right)$
  Compute the deposition rate using $\eta(\theta_{fl})$
  $\dot{m}_{f,z_i}^{(n)} \leftarrow \dot{m}_{d,z_i}^{(n)} - \dot{m}_{r,z_i}^{(n)}$
  Compute the fouling radius $r_{f,z_i}^{(n)}$, the fouling thickness $\delta_{f,z_i}^{(n)}$ and the thermal resistance $R_{f,z_i}^{(n)}$
  Evaluate the average thermal resistance $\overline{R_f^{(n)}}$
  for $m = 1$ to $m = a$ **do**
    $\alpha_m^{(n)} \leftarrow \left\lceil \dfrac{d_m^{left} + d_m^{right}}{2\Delta r} \right\rceil$
    if $\alpha_m^{(n)} = \alpha_m^{(n-1)}$ **then**
      $p_m \leftarrow p_m$
    else
      if $\alpha_m^{(n)} > b$ **then**
        $p_m \leftarrow b$ ▷ When fouling exceeds the mesh, p_m must be equal to b
      else
        $p_m \leftarrow \alpha_m^{(n)}$
      end if
    end if
    $r_{p_m,i}^{\mathrm{TOP}} \leftarrow r_{f,z_i}^{(n)}$ for all i-th discretized node associated to p_m
  end for
end for

4 Results and discussion

The numerical experiments were computationally conducted on a pipe heat exchanger constructed of stainless steel (SS) type AISI 304, with inner diameter d_{in} = 10.0 mm, outer diameter d_o = 13.2 mm, the water velocity v = 0.85 m/s, length of the pipe longitudinal-section x_L = 20 mm, and the bulk concentration of $CaCO_3$ in the water c_F = 0.2 kg/m^3. A time step of $\Delta t = 10s$ was selected and the quadrilateral size element was $\Delta z = \Delta r = 4/55$ mm. The water temperature $\theta_\infty = 27.92°\mathrm{C}$, and the temperature of the heat exchanger wall were set as $\theta_{wb} = 109.02°\mathrm{C}$. The time domain encompasses a total of 100 hours (t_∞), resulting in 36000 time steps. Table 1 summarizes all numerical parameters used in the models presented in Section 2. As the water temperature was considered constant, the fouling layer is expected to grow uniformly along z-direction for each time step. The thermophysical parameters remain unchanged at the given water temperature. Figure 3 shows the temperature at the interfaces Γ_{fl} and Γ_{fw} over time comparing its evolution in $z = 0$ mm and $z = 20$ mm. There is no material deposited on the heat exchanger walls at $t = 0$ h, leading to identical temperatures at both the interfaces Γ_{fl} and Γ_{fw} ($\theta = 46.75°\mathrm{C}$). The fouling thickness acts as an insulating layer, resulting in a gradual retreat of the Γ_{fl} interface from the heat transfer surface as it thickens. Consequently, the temperature decreases over time, as illustrated in Fig (3a), starting at $\theta = 46.75°\mathrm{C}$ and decreasing to approximately $\theta = 35.27°\mathrm{C}$ after 100 hours. Simultaneously, the temperature of Γ_{fw} increases due to the insulating effect, which restricts heat transfer. The temperature of Γ_{fw} rises to $\theta = 86.96°\mathrm{C}$, as shown in Fig (3b). Due to the asymptotic pattern associated with

fouling growth, the temperature difference diminished gradually between time steps in both scenarios, whether it increased or decreased relative to the interface.

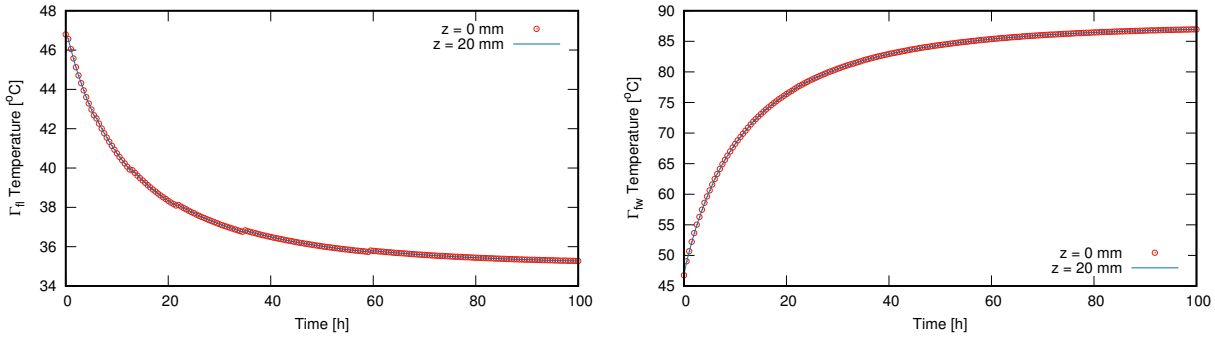

(a) Fouling-liquid layer interface

(b) Fouling-wall interface

Figure 3. Temperature behavior of the interfaces Γ_{fl} and Γ_{fw} over time: comparison at two specific points in z-direction

Figure 4 illustrates the evolution of fouling growth over space and time. Specifically, Figure 4a shows the increase in fouling thickness, reaching slightly over 0.405 mm after a 100-hour simulation. As expected, the growing fouling layer increases resistance to heat transfer, as shown in Figure 4b, although the resistance eventually reaches a limiting value. We observe that both the thickness and resistance of the fouling layer converge toward asymptotic values as the deposition and removal rates become balanced over time, $\dot{m}_{d,z_i}^{(n)} \approx \dot{m}_{r,z_i}^{(n)}$. As a result, the growth rate diminishes to zero. The average resistance $\overline{R_f^{(n)}}$ also correspond to the results depicted in Fig. 4b due to the equivalence at each spatial point over time.

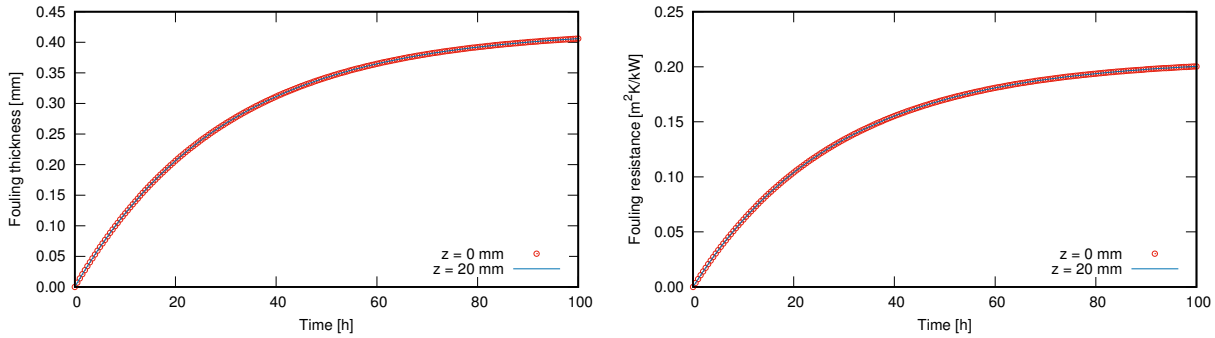

(a) Fouling thickness bahavior over time

(b) Fouling resistance over time

Figure 4. Growth of fouling thickness over space and time

The Bohnet model aims to estimate the net average of deposited particles forming a fouling layer along a heat transfer surface. In this context, the ELICAFC implementation captured the interface generated by these net average deposited particles. ELICAFC did not require remeshing, unlike ALE methods or hybrid correlated alternatives. While Eulerian schemes such as VOF or LS methods are not typically used in crystallization fouling problems and capture the interface implicitly using interpolation formulas or signed functions, ELICAFC explicitly captured the interface by directly applying the Bohnet model.

5 Conclusions

This work proposes an alternative strategy to capture the interface between a fouling layer formed by crystallization and the flowing liquid. This strategy is called an *Eulerian-like* interface-capturing approach for modeling the fouling process by crystallization (ELICAFC). A general scenario was suggested, where calcium carbonate ($CaCO_3$) is deposited on the heat exchanger walls forming a fouling layer structure. Specifically, the temperature of the fouling-liquid layer interface decreased over time, while the temperature of the fouling-wall interface increased due to the fouling layer acting as an insulating barrier. The fouling resistance increased over time due to the evolution of the fouling, and the fouling thickness reached a height of 0.4 mm. Overall, the ELICAFC results consistently align with the expected physical behavior. In forthcoming works, the ELICAFC procedure will be applied by considering the variation of water temperature and the breaking-off of calcium carbonate. Analyses of experimental scenarios documented in the literature will be addressed in future works.

Table 1. Parameters used in both the heat transfer and fouling models

Symbol	Meaning	Unit	Value	Reference
ϵ	Roughness coefficient of the pipe or fouling surface	$[\mathrm{m}]$	2×10^{-5}	Babuška et al. [5]
c_d	Crystal diameter	$[\mathrm{m}]$	30×10^{-6}	Babuška et al. [5]
k_w	Thermal conductivity of SS	$[\mathrm{W/m°K}]$	14.91811^*	Cengel and Ghajar [10]
ρ_l	Thermal conductivity of the water	$[\mathrm{W/m°K}]$	0.6116^*	Cengel and Ghajar [10]
ρ_w	Density of SS	$[\mathrm{kg/m^3}]$	7900	Cengel and Ghajar [10]
ρ_l	Density of the water	$[\mathrm{kg/m^3}]$	996.416^*	Cengel and Ghajar [10]
c_{pw}	Specific heat of SS	$[\mathrm{J/kg\,°K}]$	477.406^*	Cengel and Ghajar [10]
c_{pl}	Specific heat of the water	$[\mathrm{J/kg°K}]$	4178.832^*	Cengel and Ghajar [10]
μ_l	Dynamic viscosity of the water	$[\mathrm{kg/m\,s}]$	8.3668×10^{-4}	Cengel and Ghajar [10]
R	Real gas constant	$[\mathrm{J/kmol\,°K}]$	8314.47	Cengel and Ghajar [10]
g	Acceleration of gravity	$[\mathrm{m^2/s}]$	9.8	Cengel and Ghajar [10]
c_{pf}	Specific heat of $CaCO_3$	$[\mathrm{J/kg°K}]$	838.1493^*	Jacobs et al. [11]
k_f	Thermal conductivity of $CaCO_3$	$[\mathrm{W/m°K}]$	1.942	Müller-Steinhagen [12]
ρ_f	Density of $CaCO_3$	$[\mathrm{kg/m^3}]$	2705	Müller-Steinhagen [12]
θ_∞	Reference temperature	$[°\mathrm{K}]$	336	Müller-Steinhagen [12]
$D_{\theta_{ref}}$	Reference diffusion coefficient	$[\mathrm{m^2/s}]$	1.1456×10^{-9}	Müller-Steinhagen [12]
θ_{bo}	Temperature of boiling water	$[°\mathrm{K}]$	373.15	Müller-Steinhagen [12]
η_0	Proportionality constant	$[\mathrm{m^4/kg\,s}]$	9.8×10^{11}	Müller-Steinhagen [12]
c_s	Saturation concentration	$[\mathrm{kg/m^3}]$	0.005648436	Plummer and Busenberg [13]
E	Activation energy	$[\mathrm{J/kmol}]$	122150	Müller-Steinhagen [12]

*Values linearly interpolated at the water temperature θ_∞ based on those reported in the associated reference.

Acknowledgements. This work was supported by the *Coordenação de Aperfeiçoamento de Pessoal de Nível Superior* - Brazil (CAPES), and by CNPq 306588/2022-6.

Authorship statement. The authors hereby confirm that they are the sole liable persons responsible for the authorship of this work, and that all material that has been herein included as part of the present paper is either the property (and authorship) of the authors, or has the permission of the owners to be included here.

References

[1] M. Wörner. Numerical modeling of multiphase flows in microfluidics and micro process engineering: a review of methods and applications. *Microfluidics and nanofluidics*, vol. 12, n. 6, pp. 841–886, 2012.

[2] J. Donea, A. Huerta, J.-P. Ponthot, and A. Rodríguez-Ferran. Arbitrary Lagrangian Eulerian Methods. *Encyclopedia of computational mechanics*, 2004.

[3] M. Malú Grave, J. J. Camata, and A. L. Coutinho. Implementation of the Convected Level-set method with adaptive mesh refinement using Libmesh, 2019.

[4] R. Kasper, J. Turnow, and N. Kornev. Multiphase Eulerian–Lagrangian LES of particulate fouling on structured heat transfer surfaces. *International Journal of Heat and Fluid Flow*, vol. 79, pp. 108462, 2019.

[5] I. Babuška, R. S. Silva, and J. Actor. Break-off model for $CaCO_3$ fouling in heat exchangers. *International Journal of Heat and Mass Transfer*, vol. 116, pp. 104–114, 2018.

[6] W. M. Rohsenow, J. P. Hartnett, Y. I. Cho, and others. *Handbook of heat transfer*, volume 3. Mcgraw-hill New York, 1998.

[7] M. Bohnet. Fouling of heat transfer surfaces. *Chemical engineering & technology*, vol. 10, n. 1, pp. 113–125, 1987.

[8] R. Barrett, M. Berry, T. F. Chan, J. Demmel, J. Donato, J. Dongarra, V. Eijkhout, R. Pozo, C. Romine, and Van der H. Vorst. *Templates for the solution of linear systems: building blocks for iterative methods*. SIAM, 1994.

[9] N. C. Arruda, R. Almeida, R. Silva, and S. M. Malta. Avoiding spurious modes of time discretized operators in transport problems. *International Journal for Numerical Methods in Biomedical Engineering*, vol. 26, n. 5, pp. 609–627, 2010.

[10] Y. A. Cengel and A. J. Ghajar. Heat and mass transfer. *Penerbit McGraw-Hill Education, New York*, 2015.

[11] G. K. Jacobs, D. M. Kerrick, and K. M. Krupka. The high-temperature heat capacity of natural calcite ($CaCO_3$). *Physics and Chemistry of Minerals*, vol. 7, n. 2, pp. 55–59, 1981.

[12] H. Müller-Steinhagen. Cooling-water fouling in heat exchangers. In *Advances in heat transfer*, volume 33, pp. 415–496. Elsevier, 1999.

[13] L. N. Plummer and E. Busenberg. The solubilities of calcite, aragonite and vaterite in CO_2-H_2O solutions between 0 and 90 c, and an evaluation of the aqueous model for the system $CaCO_3$-CO_2-H_2O. *Geochimica et cosmochimica acta*, vol. 46, n. 6, pp. 1011–1040, 1982.